


# Zinc-chelating postsynaptic density-95 N-terminus impairs its palmitoyl modification

Yonghong Zhang<sup>1</sup>  | Xiaoqian Fang<sup>2</sup> | Luis Ascota<sup>1,2</sup> | Libo Li<sup>1,3</sup> | Lili Guerra<sup>2</sup> | Audrey Vega<sup>1</sup> | Amanda Salinas<sup>1</sup> | Andrea Gonzalez<sup>1</sup> | Claudia Garza<sup>1</sup> | Andrew Tsin<sup>2</sup> | Johannes W. Hell<sup>4</sup> | James B. Ames<sup>5</sup>

<sup>1</sup>Department of Chemistry, The University of Texas Rio Grande Valley, Edinburg, Texas, USA

<sup>2</sup>Department of Molecular Science, The University of Texas Rio Grande Valley, Edinburg, Texas, USA

<sup>3</sup>Key Laboratory of Green Chemical Engineering and Technology of College of Heilongjiang Province, College of Chemical and Environmental Engineering, Harbin University of Science and Technology, Harbin, China

<sup>4</sup>Department of Pharmacology, University of California, Davis, California, USA

<sup>5</sup>Department of Chemistry, University of California, Davis, California, USA

## Correspondence

Yonghong Zhang, Department of Chemistry, The University of Texas Rio Grande Valley, 1201 W. University Drive, Edinburg, TX 78539, USA.  
Email: yonghong.zhang@utrgv.edu

## Funding information

Robert A. Welch Foundation, Grant/Award Number: BX-0048

## Abstract

Chemical synaptic transmission represents the most sophisticated dynamic process and is highly regulated with optimized neurotransmitter balance. Imbalanced transmitters can lead to transmission impairments, for example, intracellular zinc accumulation is a hallmark of degenerating neurons. However, the underlying mechanisms remain elusive. Postsynaptic density protein-95 (PSD-95) is a primary postsynaptic membrane-associated protein and the major scaffolding component in the excitatory postsynaptic densities, which performs substantial functions in synaptic development and maturation. Its membrane association induced by palmitoylation contributes largely to its regulatory functions at postsynaptic sites. Unlike other structural domains in PSD-95, the N-terminal region (PSD-95NT) is flexible and interacts with various targets, which modulates its palmitoylation of two cysteines (C3/C5) and glutamate receptor distributions in postsynaptic densities. PSD-95NT contains a putative zinc-binding motif (C2H2) with undiscovered functions. This study is the first effort to investigate the interaction between  $Zn^{2+}$  and PSD-95NT. The NMR titration of <sup>15</sup>N-labeled PSD-95NT by  $ZnCl_2$  was performed and demonstrated  $Zn^{2+}$  binds to PSD-95NT with a binding affinity ( $K_d$ ) in the micromolar range. The zinc binding was confirmed by fluorescence and mutagenesis assays, indicating two cysteines and two histidines (H24, H28) are critical residues for the binding. These results suggested the concentration-dependent zinc binding is likely to influence PSD-95 palmitoylation since the binding site overlaps the palmitoylation sites, which was verified by the mimic PSD-95 palmitoyl modification and intact cell palmitoylation assays. This study reveals zinc as a novel modulator for PSD-95 postsynaptic membrane association by chelating its N-terminal region, indicative of its importance in postsynaptic signaling.

## KEYWORDS

N-terminal domain, palmitoylation, PSD-95, zinc binding

## 1 | INTRODUCTION

Chemical synaptic transmission represents the most sophisticated process which involves many key synaptic components—neurotransmitters (e.g., glutamate, zinc), synaptic receptors (AMPA- & NMDA-type receptors), scaffolding proteins, and their interactions plus association with postsynaptic membranes at synapses. This dynamic process is highly regulated and with optimized neurotransmitter balance. Imbalanced transmitters can lead to transmission impairments, even to neurological disorders. However, the underlying molecular mechanism is far from understood. Postsynaptic density protein-95 (PSD-95) belongs to the membrane-associated guanylate kinase (MAGUK) family and has been known as the major scaffolding component of the postsynaptic architecture of glutamatergic synapses. PSD-95 plays a central role in postsynaptic plasticity and stabilization of postsynaptic changes during long-term potentiation related to learning and memory.<sup>1</sup> Structurally, PSD-95 consists of three PDZ domains followed by an SH3-GK domain tandem at the C-terminal end (Figure 1). These structural domains allow PSD-95 to interact with target proteins, that is, NMDA- and AMPA-type glutamate receptors and mediate their postsynaptic targeting and localization.<sup>2–4</sup> Nevertheless, the N-terminal region (the first 71 residues preceding PDZ1) of PSD-95 (PSD-95NT) has also been demonstrated as important for its regulatory functions at postsynaptic sites through post-translational modification and/or interaction with various target proteins including calmodulin,<sup>5</sup>  $\alpha$ -actinin-1,<sup>6</sup> and CDKL5.<sup>7</sup> For example, phosphorylation of T19 destabilizes PSD-95 within the PSD, which is a critical step for AMPAR mobilization and long-term depression (LTD).<sup>8</sup> Importantly, PSD-95NT contains two cysteines (C3 and C5) that are sites for palmitoylation by the PSD-95 palmitoyl acyl transferase (PAT) essential for membrane anchoring.<sup>9</sup> The palmitoyl modification can be removed by depalmitoylation enzymes—acyl-protein thioesterase-1 (APT1). The dynamic process of palmitoylation and depalmitoylation of PSD-95 is dependent on the accumulation of PAT and APT1, but also modulated by  $\text{Ca}^{2+}$  concentration.<sup>5,10</sup> Palmitoylation, the attachment of 16-C hydrophobic chain to cysteine residues through thioester bonds, serves as a critical force to target proteins to lipids rafts of plasma membranes for protein–membrane association.<sup>11</sup>

PSD-95 mediates postsynaptic localization of AMPA- and NMDA-type receptors through its postsynaptic membrane association due to its N-terminal palmitoylation/depalmitoylation switch, which can be mediated by calmodulin upon the influx of calcium ion through ion channels.<sup>5</sup> Intriguingly, the N-terminus of PSD-95 containing two palmitoylation sites has an unnoticed putative zinc finger motif (CXCX<sub>18</sub>HX<sub>3</sub>H, Figure 1),<sup>12</sup> its function has not been discovered.

The synaptic plasticity is regulated by a variety of modulators including zinc. The local zinc concentrations at synapses may reach up to 1 mM or more.<sup>13</sup> The ionic zinc ( $\text{Zn}^{2+}$ ) highly enriched within the postsynaptic density upon release through  $\text{Ca}^{2+}$ -permeable channels is able to influence synaptic plasticity, memory formation, and nociception by regulating transmitter receptors and signal transduction pathways.<sup>14–18</sup> Moreover, intracellular zinc accumulation is a hallmark of degenerating neurons in several neurological disorders.<sup>19,20</sup> However, it remains great concerns how zinc accumulates in the synaptic vesicles of glutamatergic neurons and how it modulates neuronal excitability and synaptic plasticity. Zinc is believed to directly inhibit NMDA-sensitive glutamate-gated channels by two separate mechanisms.<sup>21</sup> Recent studies found that synaptic inhibition of NMDA receptors by zinc depends on the direct interaction between GluN2A and ZnT1- a zinc transporter.<sup>22</sup> Importantly, zinc was revealed previously to bind synapse-associated protein 102 (SAP-102)—a homolog of PSD-95, even though its precise function is not yet fully understood.<sup>23</sup> In this work, we focused on the putative zinc finger domain in PSD-95 N-terminal region and investigated, for the first time, the direct binding of  $\text{Zn}^{2+}$  with PSD-95 N-terminus and found zinc negatively modulates PSD-95 palmitoyl modification.

## 2 | RESULTS

### 2.1 | PSD-95 N-terminal domain is unstructured and highly flexible

Other than the well-defined structural domains (i.e., PDZ, SH3, GK) in PSD-95, the N-terminal region

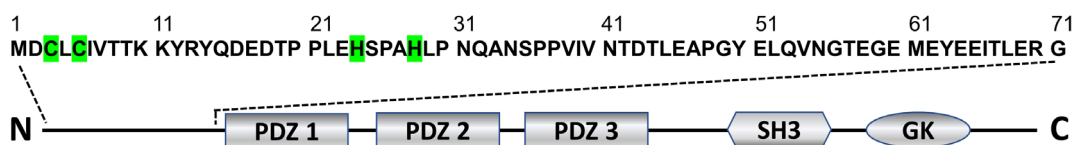


**FIGURE 1** Schematic diagram of PSD-95 and its N-terminal amino acid sequence (1–71). The putative Cys2His2-type zinc finger motif is highlighted in green

has also been discovered to be functionally important and interacts with a number of target proteins.<sup>5–7</sup> To characterize the structure and dynamics of the N-terminal domain, an NMR study was carried out recently and its backbone assignments were completed and deposited in the BMRB database (ID 50752).<sup>24</sup> Using the assigned chemical shifts, the 3D structural conformation of PSD-95NT was generated by BMRB CS-Rosetta server, which displays the 71-residue peptide adopts no defined structure and is a random coil (Figure 2a). To further verify its structural flexibility, the <sup>15</sup>N–<sup>1</sup>H-heteronuclear steady-state NOE (heteroNOE) values were measured using <sup>15</sup>N-labeled PSD-95NT. The residues at the N- and C-terminus exhibit largely negative heteroNOE values (Figure 2b), indicative of highly flexible peptide tails. All the rest of residues in the peptide demonstrate heteroNOE values at or close zero which is typical for random coil conformation. Several residues, especially in the region from residues 10 to 20, were observed with heteroNOE values up to 0.3; however, these values (less than 0.8) were far from indicating any rigid and ordered structures.

## 2.2 | Zn<sup>2+</sup> directly binds to PSD-95NT

To check if Zn<sup>2+</sup> interacts with PSD-95, specifically the putative C2H2-type zinc motif in the N-terminal region, zinc-binding experiments were carried out by intrinsic fluorescence and NMR titration. Purified PSD-95NT proteins were titrated by ZnCl<sub>2</sub> and an intrinsic fluorescence spectrum was recorded for each titration (Figure 3). The intensity of fluorescence decreases on increasing Zn<sup>2+</sup> concentration. The binding curve was obtained by plotting the relative intensity change as a function of Zn<sup>2+</sup> concentration (Figure 3 inset) for determining the binding affinity—the apparent dissociation constant (*K<sub>d</sub>*) in the micromolar range (10<sup>–6</sup>). For NMR titration, uniformly <sup>15</sup>N-labeled PSD-95NT was recorded with a 2D HSQC spectrum and then ZnCl<sub>2</sub> was gradually added into the protein solution, monitored after incubation at each stage of the titration by acquiring a 2D HSQC spectrum. Zinc ions induced significant changes of both intensity and chemical shift of HSQC peaks (Figure 4a). As many HSQC peaks disappeared in the presence of zinc ions, it is impossible to characterize Zn<sup>2+</sup>-induced changes using chemical shift perturbation. Instead, the

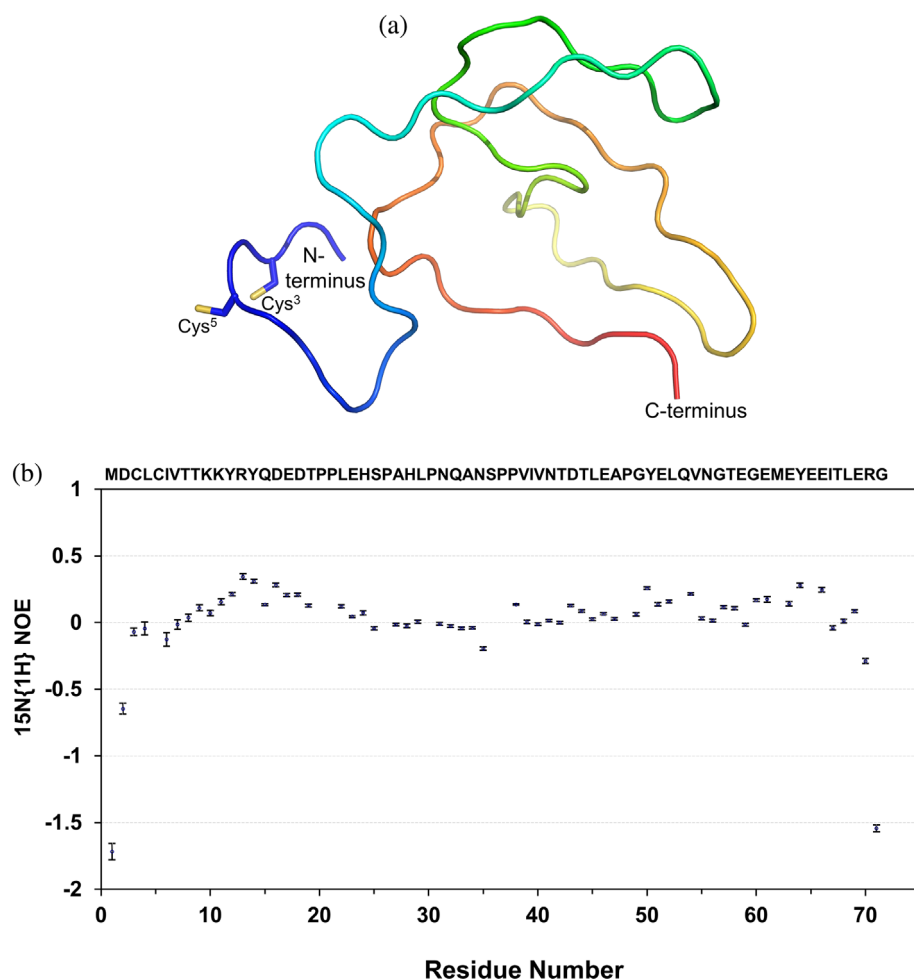
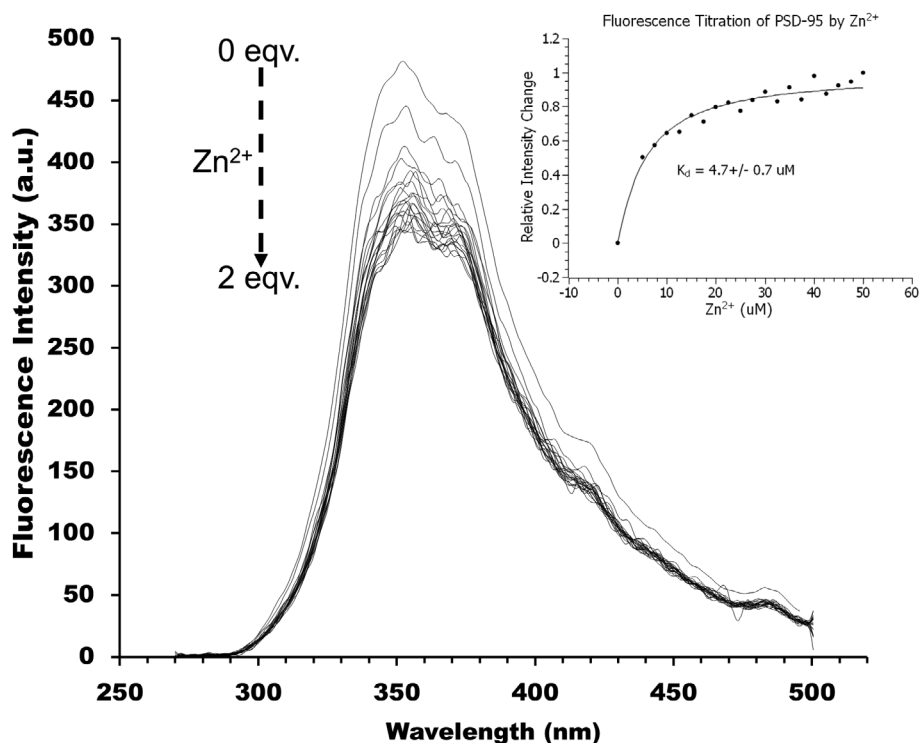


**FIGURE 2** (a) The lowest structure of PSD-95 N-terminal domain (1–71) generated by BMRB CS-Rosetta server based on the assigned chemical shifts (BMRB ID 50752). (b) PSD-95NT steady-state heteronuclear <sup>15</sup>N–(<sup>1</sup>H) NOEs. Steady-state heteronuclear <sup>15</sup>N–(<sup>1</sup>H) NOEs constitute a probe for fast dynamics of backbone N–H bonds in the hundreds of picoseconds (ps) timescale. Lower values indicate a high degree of flexibility

**FIGURE 3** Intrinsic fluorescence titration of PSD-95NT by  $Zn^{2+}$ . A series of fluorescence emission spectra were recorded for PSD-95NT protein solution when  $ZnCl_2$  was added at room temperature. The intensity of fluorescence decreases on increasing  $Zn^{2+}$  concentration. The binding curve obtained by plotting the relative intensity change as a function of  $Zn^{2+}$  concentration (inset) was fitted to give the apparent dissociation constant ( $K_d$ ) based on the equation (see *Materials and Methods*)



percentage changes in intensity of the peaks were calculated and plotted in Figure 4b. Although the intensity changes were observed for the overwhelming majority of residues (~85%), the significant changes in intensity of HSQC peaks were mainly from the first 30 residues including the putative zinc finger motif, suggesting these amino acids are likely involved in zinc binding. The apparent dissociation constant derived from NMR titration based on the relative intensity change was close to that of the fluorescence titration (Table 1), indicative of moderate affinity binding of  $Zn^{2+}$  to PSD-95NT.

### 2.3 | Structural model of $Zn^{2+}$ -bound PSD-95 N-terminal domain

To determine 3D structure of zinc-bound PSD-95NT, the first attempt following the conventional NOE-based method failed due to significantly attenuated NMR signals, for example, many peaks disappeared in the HSQC spectrum of  $^{15}N$ -labeled PSD-95NT in the presence of zinc ions, likely resulting from moderate- to low-affinity binding of  $Zn^{2+}$  to PSD-95NT and intermediate conformational exchange of PSD-95NT in free and bound state. It is, therefore, not possible to find NOEs for structure calculation. On the basis of the putative C2H2-type zinc finger motif and experimentally proved zinc binding to this motif-containing region, a

structural model of  $Zn^{2+}$ -bound PSD-95NT was generated using XPLOR-NIH by setting distance constraints between zinc and two conserved cysteines (Cys<sup>3</sup> and Cys<sup>5</sup>) and two conserved histidine residues (His<sup>24</sup> and His<sup>28</sup>) (Figure 5). The structural model displays zinc stabilizes the N-terminal domain by chelating four key residues in the C2H2-type motif, but the entire peptide chain adopts no rigid secondary structure, unlike other classic zinc fingers.<sup>12</sup>

### 2.4 | PSD-95 N-terminus binding with $Zn^{2+}$ diminished by mutation

To further test the zinc-bound PSD-95NT structural model, the following protein mutants (H24A, H28A, H24A&H28A, and C3S&C5S) were constructed and characterized for zinc binding. These mutants retain the same NMR spectrum as the wildtype protein (e.g., Figure 4a). The zinc-binding activity of PSD-95NT mutants was checked by fluorescence and NMR titration. The H24A single mutant binds to zinc(II) with ~60-fold lower affinity compared to the wildtype, whereas the two double mutants (C3S&C5S, H24A&H28A) both show ~150-fold lower zinc-binding affinities (Table 1). These results confirm that the conserved cysteines—Cys<sup>3</sup> and Cys<sup>5</sup>, and histidine residues—His<sup>24</sup> and His<sup>28</sup>, all participate in zinc(II) binding.

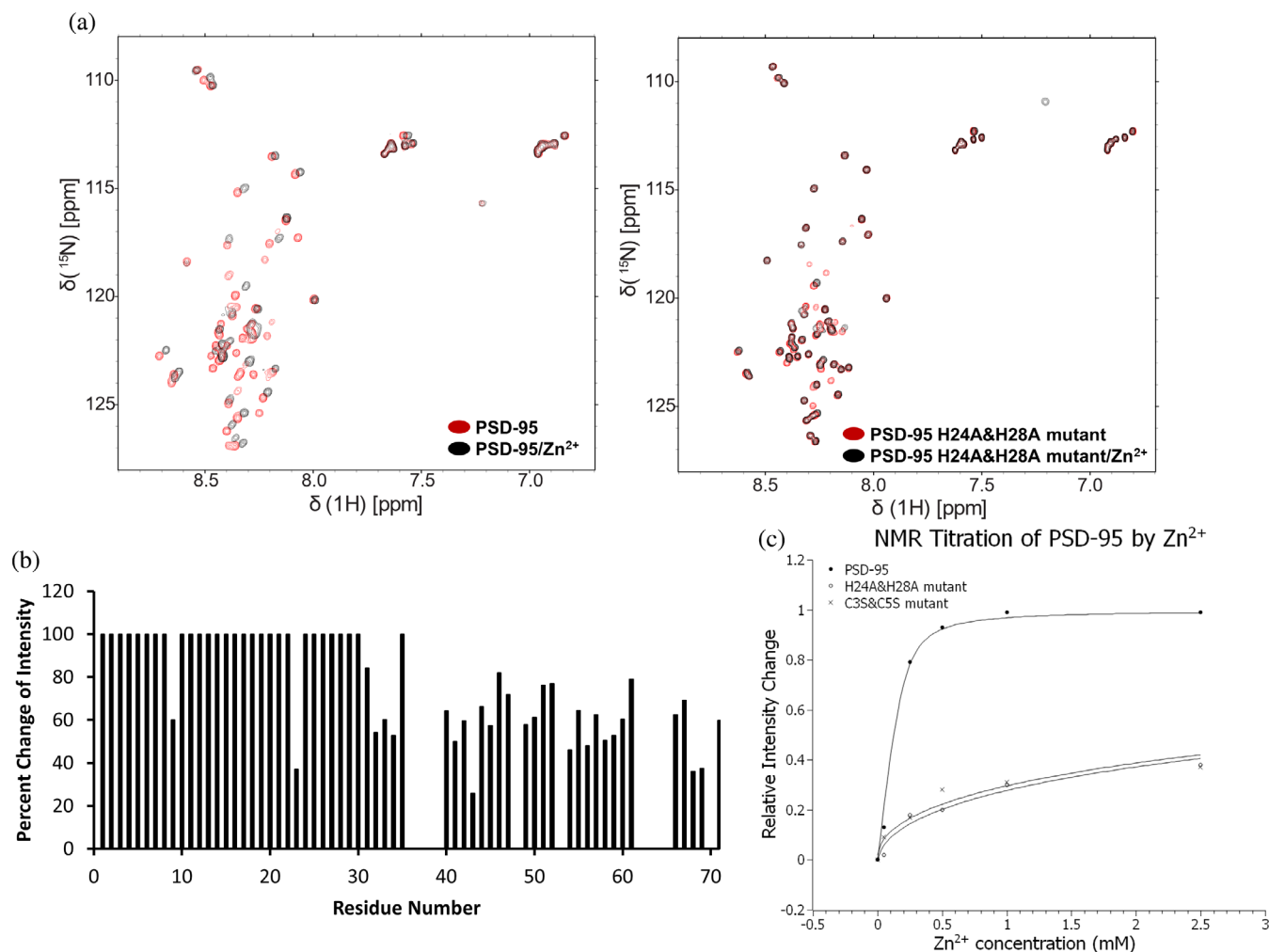


**FIGURE 4** NMR analysis of  $\text{Zn}^{2+}$  binding to PSD-95NT. (a) Overlay of 2D  $^1\text{H}$ - $^{15}\text{N}$  HSQC spectra obtained for  $^{15}\text{N}$ -labeled PSD-95NT (wildtype and H24A&H28A mutant) in the absence (red) and presence (black) of  $\text{Zn}^{2+}$ . All spectra were recorded on a Bruker Ultrashield Plus 600 MHz spectrometer at room temperature. (b)  $\text{Zn}^{2+}$ -induced percentage changes in intensity of HSQC peaks. (c) NMR titration of PSD-95NT and mutants (C3S&C5S and H24A&H28A) by  $\text{ZnCl}_2$ . The binding curve obtained by plotting the relative intensity change as a function of  $\text{Zn}^{2+}$  concentration, was fitted according to the equation (see *Materials and Methods*)

**TABLE 1** The binding affinity ( $K_d$ ) of  $\text{Zn}^{2+}$  for PSD-95 determined by fluorescence (#) and NMR titration (\*)

PSD-95/mutants	Wildtype	H24A	C3S&C5S	H24A&H28A		
$K_d$ ( $\mu\text{M}$ )	$4.7 \pm 0.7\#$	$10.5 \pm 0.7^*$	$294.4 \pm 4.7\#$	$1,100 \pm 0.3^*$	$460.7 \pm 22.7\#$	$1,500 \pm 0.3^*$

## 2.5 | Zinc binding of PSD-95NT hinders fluorescein conjugation of PSD-95 N-terminal domain

The structural model of zinc-bound PSD-95 N-terminus reveals that the two palmitoylation sites in PSD-95 (C3 and C5) are chelated by zinc(II) ion and therefore not accessible. To test whether zinc blocks the accessibility of two cysteines, the covalent attachment of a fluorescent dye (fluorescein-5-maleimide) at both Cys<sup>3</sup> and Cys<sup>5</sup> in PSD-95NT was monitored in the presence and absence of zinc

ion at the concentration of 500  $\mu\text{M}$ . This modification should mimic the attachment of palmitate at these sites.<sup>5</sup> Fluorescein-5-maleimide is a thiol-reactive molecular probe that can specifically conjugate to both C3 and C5 in PSD-95NT. The dye was added to PSD-95NT with and without  $\text{Zn}^{2+}$ . After removing unreacted dye, fluorescence emission spectra were recorded for each sample (Figure 6). Fluorescence was  $\sim 25\%$  less following incubation in the presence of 0.5 mM  $\text{Zn}^{2+}$  compared with no  $\text{Zn}^{2+}$ . These results indicate that zinc decreases the conjugation efficiency of fluorescein dye to PSD-95, likely due to blocking

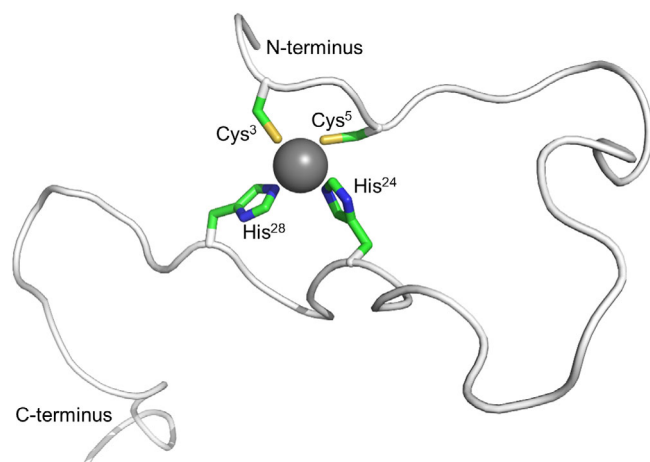


**FIGURE 5** Structural model of zinc-chelating PSD-95 N-terminal domain. The sidechains of two cysteines (Cys<sup>3</sup>, Cys<sup>5</sup>) and two histidines (His<sup>24</sup>, His<sup>28</sup>) are highlighted in green

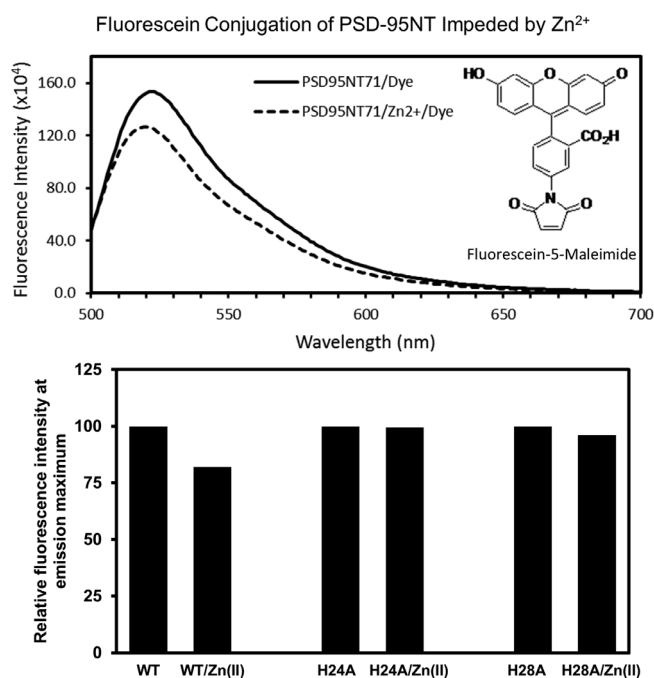


**FIGURE 6** Fluorescein-conjugated modification of PSD-95 is impeded by Zn<sup>2+</sup> binding. Fluorescence spectrum (upper panel) and relative fluorescence intensity at emission maximum (lower panel) of fluorescein-conjugated PSD-95 and mutants- H24A and H28A in the absence and presence of Zn<sup>2+</sup>. All samples contain the same concentration of PSD-95 (1–71) (75 μM). A baseline correction is performed for all fluorescence data

the accessibility of two cysteines. PSD-95 will spend some fraction of time free of zinc ion even in the presence of stoichiometric amounts of zinc, which would allow fluorescein conjugation of PSD-95 to build up over time and could explain partial rather than full block of fluorescein attachment. Compared to the wildtype, however, H24A

and H28A mutants with much lower binding affinity to Zn<sup>2+</sup> demonstrated almost no fluorescence change even in the presence of Zn<sup>2+</sup> (0.5 mM) (Figure 6). The result suggests that zinc loses its capacity of blocking the fluorescein accessibility of the two cysteines.

## 2.6 | Zn<sup>2+</sup> treatment impairs PSD-95 palmitoylation in HEK293 cells

To test in intact cells whether Zn<sup>2+</sup> treatment negatively modulates PSD-95 palmitoylation, HEK293 cells were transfected with PSD-95 and incubated for 48 hr. After the treatment with Zn<sup>2+</sup>, the cells along with the control groups were subjected to palmitoylation assay (see *Experimental Procedures*). Under basal condition, PSD-95 presented clearly a considerable level of palmitoylation in HEK293 cells (Figure 7). Zn<sup>2+</sup> treatment significantly reduced palmitoylation of PSD-95 with about 50% decrease compared to the control, although it did not change the overall protein level. However, Zn<sup>2+</sup> treatment had much less effect on the palmitoylation of PSD-95 mutation of histidine residue participating in the Zn<sup>2+</sup> coordination (Figure 7). These results suggest that binding of Zn<sup>2+</sup> to the N-terminus of PSD-95 shifts PSD-95 toward its depalmitoylation state but the mutations which weakened the binding, eliminate the inhibitory effect of Zn<sup>2+</sup> on the palmitoylation.

## 3 | DISCUSSION

### 3.1 | PSD-95 N-terminal region is a crucial functional domain

As a major scaffold protein of PSD-MAGUK family, PSD-95 is enriched at glutamatergic synapses and acts as a central organizer of postsynaptic signaling complexes comprising glutamate receptors, ion channels, cytoskeletal elements, and so on, at postsynaptic sites.<sup>25–27</sup> Its regulatory functions have been well understood,<sup>28</sup> which are exerted through its multiple structural domains plus unstructured regions/loops/hooks as a structural integrity functioning cooperatively. Of its multiple functions at postsynaptic sites, PSD-95 membrane association via its N-terminal palmitoylation and its regulation play critical roles in trafficking and anchoring glutamate receptors to postsynaptic membrane surfaces,<sup>29</sup> indicative of the importance of the N-terminal region preceding the first structured domain-PDZ1. Structurally, this region is intrinsically disordered based on NMR structural studies (Figure 2).<sup>24</sup> The structural flexibility of this N-terminal segment facilitates its post-translational modification—palmitoylation and phosphorylation,<sup>8,9,30</sup>

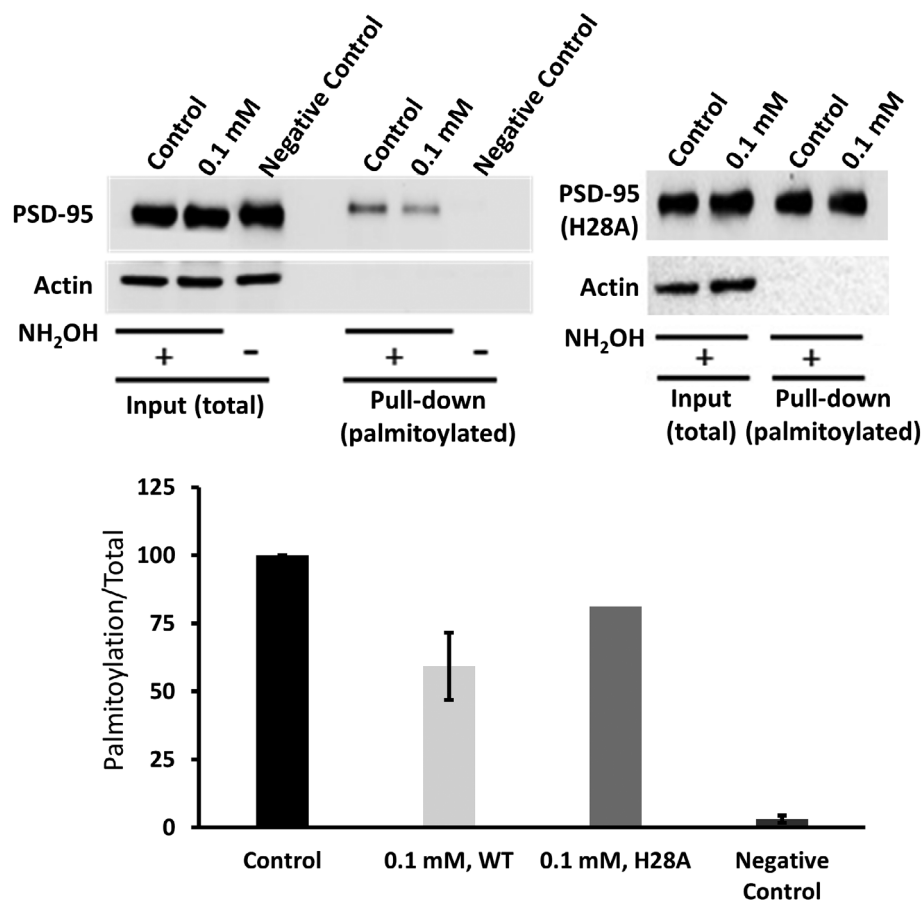


**FIGURE 7**  $Zn^{2+}$  treatment reduces PSD-95 palmitoylation in HEK-293 cells but has less effect on histidine mutation. HEK293 cells were transfected with pGW1-PSD-95 (wildtype or histidine mutation). After 48 hr, cells were treated with vehicle (Control) or 0.1 mM  $ZnCl_2$  for 5 min and extracted. NEM was added to alkylate free SH groups on Sys. Palmitoylated Cys were deacylated with hydroxylamine ( $NH_2OH$ ), and newly available SH groups biotinylated for pull-down with streptavidin, following by immunoblotting for PSD-95. Omission of  $NH_2OH$  prevented pull-down of PSD-95 and no palmitoylated PSD-95 detected (right lane, negative control) indicating the specificity of this procedure.  $Zn^{2+}$  treatment decreased wildtype PSD-95 palmitoylation level to about 50% compared to the control, but histidine mutation only to 85%

and/or interaction with multiple binding partners.<sup>5-7</sup> These diverse interactions largely contribute to PSD-95 N-terminus-originated regulation functions at postsynaptic sites.<sup>5,6</sup> It is not unusual for a protein with an intrinsically disordered N- or C-terminal segment that is able to interact with many different binding partners to exert multiple regulation functions, for example, p53.<sup>31</sup> Interestingly, PSD-MAGUK protein family (PSD-95, PSD-93, SAP-97, SAP-102) shares structures and functions, but also contains different N-termini and unique features, for example, palmitoylation is a feature particular to PSD-95 and PSD-93, but not to SAP-102 and Sap-97.<sup>23</sup> These results suggested the N-terminal region is an important functional domain. In this study, we focus on the structural and functional analysis of  $Zn^{2+}$  binding to the N-terminus of PSD-95 because this region and especially its palmitoylation are critical for targeting PSD-95 to postsynaptic membranes.

### 3.2 | Zinc finger motif at the PSD-95 N-terminus

PSD-95 N-terminal region contains posttranslational modification sites—two cysteines (C3 and C5) for

palmitoylation and several residues of threonine/serine (T8, T19, S25, S35, T47, etc.) for phosphorylation which identified through MS-MS studies.<sup>30</sup> It also has a calmodulin binding motif between residues 2 and 16.<sup>5</sup> Following previous studies that N-terminal cysteines in SAP-102 bind tightly to zinc,<sup>23</sup> we took a closer look at the N-terminal amino acid sequence and found a putative C2H2-like zinc finger motif- **CXC(X)<sub>18</sub>HXXXH** formed by two cysteines (C3, C5) and two histidines (H24, H28). However, this is not a typical C2H2 motif because only one residue exists between two cysteines.<sup>12</sup> Unlike other classic zinc finger motifs, the zinc-binding affinity to PSD-95NT is in the order of micromolar range (Table 1), weaker than classical zinc finger motifs in the lower nanomolar range. Because of the weak zinc binding, it is difficult to directly determine the 3D structure of zinc-bound PSD-95NT by following conventional NOE-based approaches. A structure model of zinc-bound PSD-95NT was generated indicating zinc ion coordinates cysteines and histidines in a tetrahedral array (Figure 5). This model structure is different from a classic C2H2 zinc finger domain which usually comprises a  $\beta$ -hairpin and an  $\alpha$ -helix in a left-handed  $\beta\beta\alpha$  folding pattern.<sup>12</sup> The <sup>15</sup>N—<sup>1</sup>H heteroNOE data (Figure 2b) suggested that the regions (amino acids from 1 to 8, 23 to 35) comprising

two cysteines and two histidines are very flexible, which facilitates zinc binding in a dynamic manner, and likely fits the dynamic regulatory function of zinc against PSD-95 at postsynaptic sites. Our study provides the first evidence to demonstrate directly binding of zinc with PSD-95 at zinc-binding sites which overlaps the palmitoylation sites. This C2H2-like zinc-binding domain has not been noticed previously.

### 3.3 | $Zn^{2+}$ negatively modulates palmitoylation of PSD-95

In this study, we provide, for the first time, the evidences indicating that  $Zn^{2+}$  binds the amino-terminal region of PSD-95 (Figures 1 and 5), and we propose a model to explain how ionic zinc chelates the zinc finger domain including two cysteines at positions 3 and 5 near the N-terminus and prevents PSD-95 palmitoylation (Figure 8). Under basal conditions, PSD-95 is attached to the postsynaptic membrane through palmitoylation of two cysteines (C3/C5), where it stabilizes AMPA-type glutamate receptors through the direct interaction with their auxiliary TARP subunit,<sup>32</sup> and NMDA-type receptors by directly binding to the PDZ domain in the C-termini tail of GluN2 subunits,<sup>33–35</sup> or inducing the degradation of STEP<sub>61</sub> at postsynaptic sites.<sup>36</sup> However,  $Zn^{2+}$  influx through voltage-sensitive  $Ca^{2+}$  channels,<sup>37</sup> NMDA channels,<sup>38</sup> or  $Ca^{2+}$ -permeable AMPA/kainate channels,<sup>39</sup> decreases palmitoylation of PSD-95 as  $Zn^{2+}$  chelates two cysteines to block the palmitoyl modification and shifts the dynamic equilibrium of the constitutive palmitoylation/depalmitoylation cycle toward the latter (Figure 8). In this manner,  $Zn^{2+}$  promotes PSD-95 dissociation from the postsynaptic membrane, which induces destabilization of NMDA- and AMPA-type receptors. This is a new and alternative mechanism of zinc induced inhibition of NMDA- and AMPA-type receptors. On the other hand,

PSD-95 can also chelate zinc ion when intracellular  $Zn^{2+}$  levels become excessively high and function as an intracellular modulator of cytosolic zinc.

In this study, we identified a C2H2-like zinc-binding domain in PSD-95NT and revealed zinc as a modulator for PSD-95 palmitoylation which represents a novel, unrecognized mechanism. However, zinc-bound PSD-95NT may have other functions with the involvement in mediating protein–protein interaction as a regulator in cell signaling, which remain elusive since zinc fingers usually perform a broad range of functions in various cellular processes.<sup>12</sup>

## 4 | MATERIALS AND METHODS

### 4.1 | Recombinant DNA plasmids

The genes encoding PSD-95 N-terminal domain (PSD-95NT, residues 1–71) were subcloned into pGEX-4T3 and pET24b vector for the construction of two recombinant PSD-95NT DNA plasmids, respectively.<sup>5</sup> The recombinant DNA plasmids were used as templates to construct PSD-95NT mutation plasmids including Y12W, H24A, H28A, C3S&C5S, and H24A&H28A, by using Site-Directed Mutagenesis Kits (QuikChange II, Agilent). For PSD-95 palmitoylation assay in HEK-293 cells, pGW1-PSD-95 plasmids and histidine mutation were used, and all mutations were generated by using Site-Directed Mutagenesis Kits (QuikChange II XL, Agilent). All DNA plasmids were checked and verified by DNA sequencing (Functional Biosciences). GST-tagged full-length PSD-95 recombinant DNA plasmid was also used as described previously.<sup>6</sup>

### 4.2 | Protein expression and purification

PSD-95 and PSD-95NT plasmids were transformed into One Shot™ BL21(DE3) Chemically Competent

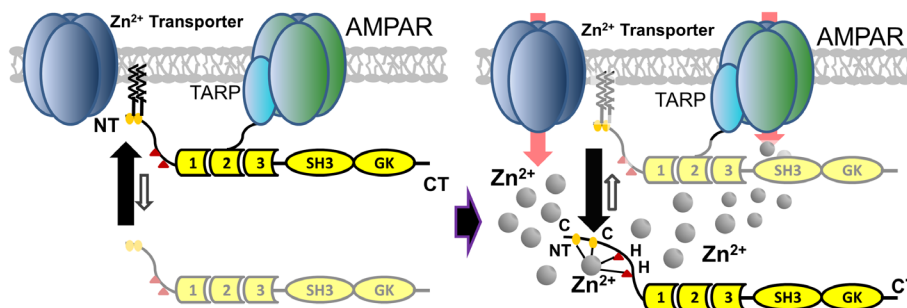


**FIGURE 8** Model of  $Zn^{2+}$ -induced postsynaptic release of PSD-95. Left: Under basal conditions, PSD-95 (yellow) is attached to the postsynaptic site through palmitoylation of Cys<sup>3</sup> and Cys<sup>5</sup>. It keeps AMPA-type glutamate receptors (green) via binding to the C-termini of their auxiliary TARP subunits (cyan) at postsynaptic sites. Right:  $Zn^{2+}$  influx through AMPA receptors or  $Zn^{2+}$  transporter results in chelating PSD-95NT to prevent re-palmitoylation. Consequently, a fraction of PSD-95 leaves the postsynaptic site



*Escherichia coli* (Invitrogen™, C600003) for protein over-expression in Lysogeny broth (LB) medium (unlabeled proteins) or M9 minimal media supplemented with  $^{15}\text{NH}_4\text{Cl}$  or  $^{15}\text{NH}_4\text{Cl}/^{13}\text{C}$ -glucose for single- or double-labeled proteins. An overnight culture (10 ml) of *E. coli* cells with recombinant DNA plasmids of PSD-95 (full-length or N-terminal domain) was diluted into 1 L fresh media (LB or M9) with antibiotic (ampicillin for GST-tagged plasmids, kanamycin for His-tagged plasmids). The culture was grown at 37°C to an optical density ( $\text{Abs}_{600}$ ) of 0.6, and then 0.5 ml isopropyl  $\beta$ -D-1-thiogalactopyranoside (IPTG, 1 M) was added to induce the overexpression of target protein for 4 hr. The bacteria were finally harvested to cell pellets by centrifugation (Beckman Coulter Avanti J-E Centrifuge). Recombinant fusion protein (GST- or His-tagged PSD-95 or PSD-95NT) was purified from the cell pellets following standard affinity purification protocol on GST column<sup>40</sup> or Ni-NTA column.<sup>41</sup> The GST tag of PSD-95 fusion protein was removed by thrombin digestion (Biotinylated, Millipore), and PSD-95 (full-length or N-terminal domain) was loaded onto a size-exclusion column (HiLoad 26/600 Superdex 75 pg) on a GE Healthcare AKTA pure 25 L1 system for further purification. Similarly, His-tagged PSD-95NT from Ni-NTA column was purified by gel-filtration chromatography.

### 4.3 | NMR experiments

The purified isotopic labeled PSD-95NT protein was exchanged into NMR buffer (pH 7.2) containing 20 mM Tris- $d_{11}$  with 100 mM NaCl, 5 mM tri(2-carboxyethyl) phosphine (TCEP), and 92%  $\text{H}_2\text{O}/8\%$   $\text{D}_2\text{O}$  using a Millipore Amicon Ultra Centrifuge Filter Ultracel-3 K (Millipore #UFC900324, 3 kDa cut-off). The protein sample was concentrated to about 0.5 mM in 0.5 ml and transferred into an NMR tube after removal of any precipitates by centrifugation. All NMR experiments were performed at room temperature using a Bruker Ultrashield Plus 600 MHz spectrometer. The  $^{15}\text{N}$ – $^1\text{H}$  two-dimensional HSQC spectra were recorded using 256 (F1)  $\times$  1024 (F2) complex points. The steady-state  $^{15}\text{N}$ –( $^1\text{H}$ ) heteronuclear NOE experiments were performed using standard pulse sequence as previously described.<sup>42</sup> To allow heteronuclear NOE evolution,  $^{15}\text{N}$ –( $^1\text{H}$ ) steady-state NOE values were determined with two different data sets, one acquired with no initial proton saturation and the other with initial proton saturation. The proton saturation period was set to 3 s. The heteronuclear NOE experiments were repeated three times to calculate the average and standard deviation of the NOE values. The NMR data were processed using

NMRPipe (<https://www.ibbr.umd.edu/nmrpipe/>) and analyzed using Sparky (<https://nmrfam.wisc.edu/nmrfam-sparky-distribution/>).

### 4.4 | $\text{Zn}^{2+}$ -bound PSD-95NT structure modeling

The structure of  $\text{Zn}^{2+}$ -bound PSD-95NT was generated by XPLOR-NIH, using distance restraints based on Cys2-His2 zinc finger motif in PSD-95 amino acid sequence (Cys<sup>3</sup>/Cys<sup>5</sup>, His<sup>24</sup>/His<sup>28</sup>). The distance constraints included four fixed distances from zinc ion to PSD-95NT where the zinc–sulfur ( $\text{S}^\gamma$ ) and zinc–nitrogen ( $\text{N}^{\epsilon 2}$ ) bond length were set to 2.3 and 2.0 Å, respectively.<sup>43,44</sup> Other distance constraints involved in structure modeling were the distance between two sulfur atoms ( $\text{S}^\gamma$ – $\text{S}^\gamma$ ) of two Cys residues which was set to 3.7 Å, and two nitrogen atoms ( $\text{N}^{\epsilon 2}$ – $\text{N}^{\epsilon 2}$ ) of two His residues which was set to 3.3 Å, and four distances between sulfur ( $\text{S}^\gamma$ ) of Cys and nitrogen ( $\text{N}^{\epsilon 2}$ ) of His, that is, Cys<sup>3</sup> and His<sup>24</sup>/His<sup>28</sup>, Cys<sup>5</sup> and His<sup>24</sup>/His<sup>28</sup>, which was set to 3.5 Å. Structure calculation were performed following similar protocol as described previously.<sup>45</sup> The lowest energy structure was selected as the structure model.

### 4.5 | Fluorescence titration

Titration of PSD-95NT and mutants by  $\text{ZnCl}_2$  (0.1 M, Sigma-Aldrich) were performed on a PerkinElmer Precisely LS55 Luminescence Spectrometer at room temperature. Purified PSD-95NT proteins (wildtype and mutants) were first treated with DTT to reduce all Cys residues and then exchanged to Tris buffer (20 mM Tris, 100 mM NaCl, pH 7.4). The titration was performed by gradually adding  $\text{ZnCl}_2$  into to the protein solution (21  $\mu\text{M}$ ) with a 2.5-fold molar excess of  $\text{Zn}^{2+}$ . The protein samples were experimentally measured by fluorescence spectroscopy in the absence and presence of  $\text{Zn}^{2+}$ . For fluorescence measurement, the excitation wavelength was set to 268 nm, and the emission spectra were recorded from 270 to 500 nm (excitation slit = 10 nm, emission slit = 10 nm, scan speed = 500 nm/min, and number of accumulation scans = 5). The binding affinity ( $K_d$ ) was determined by data analysis of fluorescence intensity change versus the concentration change of  $\text{Zn}^{2+}$  using SciDAVis program according to the following equation<sup>46</sup>:

$$x = \frac{(K_d + [L] + [P]) \pm \sqrt{(K_d + [L] + [P])^2 - 4[P][L]}}{2[P]}$$

where  $x$  is the relative intensity changes,  $[T]$  and  $[P]$  are the concentrations of titrant (T) and protein (P).

#### 4.6 | Fluorescein conjugation assay

Fluorescein conjugation assay was performed on an Edinburgh Instruments FLS980 fluorimeter system equipped with a Xenon lamp as an excitation source and a TE-cooled photo-multiplier tube (Hamamatsu, Model R928P) for emission detection. Fluorescent dye (fluorescein-5-maleimide) was ordered from Life Technologies (<http://invitrogen.com>). For fluorescein conjugation assay, PSD-95NT proteins (wildtype or mutants) (cysteines were reduced by treatment with TCEP) were exchanged to Tris buffer (20 mM Tris, 100 mM NaCl, pH 7.4), and the concentration was determined by UV absorption at 276 nm. The fluorescein dyes dissolved in DMSO were added to the solutions (75  $\mu$ M) of PSD-95NT (wildtype or mutants) in the absence and presence of  $Zn^{2+}$  (500  $\mu$ M). All reaction mixtures were incubated at room temperature for 1 hr, and then immediately passed over pre-equilibrated Zeba spin desalting columns (7K MWCO, Thermo SCIENTIFIC) to remove the excess/unconjugated fluorescein dyes. SDS-PAGE protein gel check confirmed that all proteins were retained in the filter solutions. Fluorescence emission spectra of all filtered protein solutions were recorded at room temperature between 500 and 750 nm with excitation at 496 nm. The excitation and emission slit widths were both 5 nm. Data were collected at 1.0 nm increments with 1.0 s integration time, and spectra were corrected by digital subtraction of buffer blanks.

#### 4.7 | PSD-95 palmitoylation assay

HEK293 cells were cultured in 60 mm culture dishes at the density of  $6 \times 10^4$  cells/cm<sup>2</sup> with Dulbecco's Modified Eagles Media (DMEM) supplemented with 10% fetal bovine serum. HEK293 cells were transfected with PSD-95 plasmid DNA (pGW1-PSD-95, 1.5  $\mu$ g) using LipiD293<sup>TM</sup> DNA in vitro transfection reagent (Ver. II, SigmaGen, Ijamsville, MD). After incubated with the plasmid DNA and transfection agents, cells were incubated with fresh DMEM supplemented with 10% fetal bovine serum and maintained for 48 hr before experiment. Palmitoylation assay was performed as described<sup>47</sup> with modifications. After treatment, cells were rinsed in PBS and lysed in 0.1 ml of lysis buffer (LB, 150 mM NaCl, 50 mM Tris-HCl, pH 7.5, 5 mM EDTA, protease inhibitor cocktail [Santa Cruz], 0.2 mM PMSF) containing 2% SDS and 25 mM N-ethyl-maleimide (NEM, Sigma).

After breaking open cells with burst sonication and extracting at 37°C for 15 min, lysates were diluted 10-fold with LB containing 2% Triton X-100 and 25 mM NEM followed by incubation at 4°C for 1 hr. The lysates were centrifuged at 16,000 $\times$ g for 10 min at 4°C and protein concentrations were measured using BCA assay (Thermo Scientific). Supernatants (150  $\mu$ g) were chloroform-methanol (CM) precipitated and protein pellets were solubilized in 0.2 ml of LB containing 4% SDS (4SB) and 25 mM NEM and incubated at 37°C for 10 min. And then the samples were diluted five-fold with LB containing 0.2% Triton X-100 and 1 mM NEM and incubated at 4°C overnight with end-to-end rotation. Excess NEM was removed by three sequential CM precipitations and protein pellets were dissolved in 0.2 ml of 4SB. Hydroxylamine (NH<sub>2</sub>OH) is a reducing agent and used to cleave thioester bonds, which exposing sulfur for biotin binding. Each sample was diluted five-fold by adding HA buffer (0.7 M hydroxylamine, pH 7.4, 0.2% Triton-100, protease inhibitor cocktail, 0.2 mM PMSF) with 1 mM EZ-link HPDP-biotin and incubated at room temperature for 1 hr. In the negative control group, Tris was used to replace NH<sub>2</sub>OH and palmitoylate groups were not removed and could not be detected by biotinylation. After 1-hr incubation, samples were subjected to CM precipitation. Resulting protein pellets were dissolved in 0.2 ml of 4SB, diluted five-fold with addition of low-HPDP-biotin buffer (LB containing 0.2% Triton X-100 and 0.2 mM HPDP-biotin), and incubated at room temperature for 1 hr with end-to-end rotation. Unreacted HPDP-biotin was removed by CM precipitation and protein pellets were dissolved in 0.1 ml of 2SB (150 mM NaCl, 5 mM EDTA, 2% SDS). And then samples were diluted two-fold in LB containing 0.2% Triton X-100 and 10% (v/v) of each sample was taken as input. The remaining samples were further diluted five-fold in LB containing 0.2% Triton X-100 and incubated with Streptavidin Plus UltraLink<sup>TM</sup> Resin (Thermo Scientific) at room temperature for 90 minutes. After washing the beads, the bound proteins were eluted in SDS-PAGE sample buffer. Both inputs and eluates were analyzed by SDS-PAGE and immunoblotting.

#### ACKNOWLEDGMENTS

We would like to thank Mr Thomas Eubanks for NMR technical support at UTRGV and Dr Bhupendra Srivastava for his assistance with partial fluorescence measurement. This work was supported by a UTRGV FRC award to Yonghong Zhang. The Department of Chemistry at UTRGV is grateful for the generous support provided by a Departmental Grant from the Robert A. Welch Foundation (grant number BX-0048).

## CONFLICT OF INTEREST

The authors declare that they have no conflict of interest.

## AUTHOR CONTRIBUTIONS

**Yonghong Zhang:** Conceptualization (lead); data curation (lead); formal analysis (lead); investigation (lead); methodology (lead); project administration (lead); resources (lead); software (lead); supervision (lead); validation (lead); visualization (lead); writing – original draft (lead); writing – review and editing (lead). **Xiaoqian Fang:** Data curation (equal); methodology (equal); supervision (equal); validation (equal); visualization (equal); writing – review and editing (equal). **Luis Acosta:** Data curation (supporting). **Libo Li:** Data curation (supporting). **Lili Guerra:** Data curation (supporting). **Audrey Vega:** Data curation (supporting). **Amanda Salinas:** Data curation (supporting). **Andrea Gonzalez:** Data curation (supporting). **Claudia Garza:** Data curation (supporting). **Andrew Tsin:** Resources (equal). **Johannes W. Hell:** Writing – review and editing (supporting). **James B. Ames:** Writing – review and editing (supporting).

## ORCID

Yonghong Zhang  <https://orcid.org/0000-0002-7305-9295>

## REFERENCES

1. Cho KO, Hunt CA, Kennedy MB. The rat brain postsynaptic density fraction contains a homolog of the *Drosophila* discs-large tumor suppressor protein. *Neuron*. 1992;9:929–942.
2. Kim E, Sheng M. PDZ domain proteins of synapses. *Nat Rev Neurosci*. 2004;5:771–781.
3. Rademacher N, Kurovka B, Kunde SA, Wahl MC, Freund C, Shoichet SA. Intramolecular domain dynamics regulate synaptic MAGUK protein interactions. *Elife*. 2019;8:e41299.
4. Xu W. PSD-95-like membrane associated guanylate kinases (PSD-MAGUKs) and synaptic plasticity. *Curr Opin Neurobiol*. 2011;21:306–312.
5. Zhang Y, Matt L, Patriarchi T, et al. Capping of the N-terminus of PSD-95 by calmodulin triggers its postsynaptic release. *EMBO J*. 2014;33:1341–1353.
6. Matt L, Kim K, Hergarden AC, et al. Alpha-actinin anchors PSD-95 at postsynaptic sites. *Neuron*. 2018;97:1094–1109.
7. Zhu YC, Li D, Wang L, et al. Palmitoylation-dependent CDKL5-PSD-95 interaction regulates synaptic targeting of CDKL5 and dendritic spine development. *Proc Natl Acad Sci U S A*. 2013;110:9118–9123.
8. Nelson CD, Kim MJ, Hsin H, Chen Y, Sheng M. Phosphorylation of threonine-19 of PSD-95 by GSK-3 $\beta$  is required for PSD-95 mobilization and long-term depression. *J Neurosci*. 2013;33:12122–12135.
9. Fukata M, Fukata Y, Adesnik H, Nicoll RA, Brecht DS. Identification of PSD-95 palmitoylating enzymes. *Neuron*. 2004;44:987–996.
10. Conibear E, Davis NG. Palmitoylation and depalmitoylation dynamics at a glance. *J Cell Sci*. 2010;123:4007–4010.
11. Matt L, Kim K, Chowdhury D, Hell JW. Role of palmitoylation of postsynaptic proteins in promoting synaptic plasticity. *Front Mol Neurosci*. 2019;12:8.
12. Krishna SS, Majumdar I, Grishin NV. Structural classification of zinc fingers: Survey and summary. *Nucleic Acids Res*. 2003;31:532–550.
13. Frederickson CJ, Suh SW, Silva D, Frederickson CJ, Thompson RB. Importance of zinc in the central nervous system: The zinc-containing neuron. *J Nutr*. 2000;130:1471S–1483S.
14. Kay AR, Toth K. Influence of location of a fluorescent zinc probe in brain slices on its response to synaptic activation. *J Neurophysiol*. 2006;95:1949–1956.
15. Paoletti P, Vergnano AM, Barbour B, Casado M. Zinc at glutamatergic synapses. *Neuroscience*. 2009;158:126–136.
16. Vergnano AM, Rebola N, Savtchenko LP, et al. Zinc dynamics and action at excitatory synapses. *Neuron*. 2014;82:1101–1114.
17. Koh JY, Lim JS, Byun HR, Yoo MH. Abnormalities in the zinc-metalloprotease-BDNF axis may contribute to megalencephaly and cortical hyperconnectivity in young autism spectrum disorder patients. *Mol Brain*. 2014;7:64.
18. Zhu J, Shao CY, Yang W, et al. Chronic zinc exposure decreases the surface expression of NR2A-containing NMDA receptors in cultured hippocampal neurons. *PLoS One*. 2012;7:e46012.
19. Yang Y, Jing XP, Zhang SP, et al. High dose zinc supplementation induces hippocampal zinc deficiency and memory impairment with inhibition of BDNF signaling. *PLoS One*. 2013;8:e55384.
20. Sindreu C, Bayés À, Altafaj X, Pérez-Clausell J. Zinc transporter-1 concentrates at the postsynaptic density of hippocampal synapses. *Mol Brain*. 2014;7:16.
21. Amico-Ruvio SA, Murthy SE, Smith TP, Popescu GK. Zinc effects on NMDA receptor gating kinetics. *Biophys J*. 2011;100:1910–1918.
22. Krall RF, Moutal A, Phillips MB, et al. Synaptic zinc inhibition of NMDA receptors depends on the association of GluN2A with the zinc transporter ZnT1. *Sci Adv*. 2020;6:eabb1515.
23. El-Husseini AE, Topinka JR, Lehrer-Graiwer JE, et al. Ion channel clustering by membrane-associated guanylate kinases. Differential regulation by N-terminal lipid and metal binding motifs. *J Biol Chem*. 2000;275:23904–23910.
24. Zhang Y, Hell JW, Ames JB. Chemical shift assignments of the N-terminal domain of PSD95 (PSD95-NT). *Biomol NMR Assign*. 2021. <https://doi.org/10.1007/s12104-021-10028-5>. Online ahead of print
25. Topinka JR, Brecht DS. N-terminal palmitoylation of PSD-95 regulates association with cell membranes and interaction with K<sup>+</sup> channel Kv1.4. *Neuron*. 1998;20:125–134.
26. Dosemeci A, Makusky AJ, Jankowska-Stephens E, Yang X, Slotta DJ, Markey SP. Composition of the synaptic PSD-95 complex. *Mol Cell Proteomics*. 2007;6:1749–1760.
27. Chen X, Levy JM, Hou A, et al. PSD-95 family MAGUKs are essential for anchoring AMPA and NMDA receptor complexes at the postsynaptic density. *Proc Natl Acad Sci U S A*. 2015;112:E6983–E6992.
28. Keith D, El-Husseini A. Excitation control: Balancing PSD-95 function at the synapse. *Front Mol Neurosci*. 2008;1:4.

29. Jeyifous O, Lin EI, Chen X, et al. Palmitoylation regulates glutamate receptor distributions in postsynaptic densities through control of PSD95 conformation and orientation. *Proc Natl Acad Sci U S A*. 2016;113:E8482–E8491.
30. Pedersen SW, Albertsen L, Moran GE, et al. Site-specific phosphorylation of PSD-95 PDZ domains reveals fine-tuned regulation of protein-protein interactions. *ACS Chem Biol*. 2017;12:2313–2323.
31. Krois AS, Dyson HJ, Wright PE. Long-range regulation of p53 DNA binding by its intrinsically disordered N-terminal transactivation domain. *Proc Natl Acad Sci U S A*. 2018;115:E11302–E11310.
32. Bats C, Groc L, Choquet D. The interaction between stargazin and PSD-95 regulates AMPA receptor surface trafficking. *Neuron*. 2007;53:719–734.
33. Chung HJ, Huang YH, Lau LF, Huganir RL. Regulation of the NMDA receptor complex and trafficking by activity-dependent phosphorylation of the NR2B subunit PDZ ligand. *J Neurosci*. 2004;24:10248–10259.
34. Kornau HC, Schenker L, Kennedy M, Seeburg P. Domain interaction between NMDA receptor subunits and the postsynaptic density protein PSD-95. *Science*. 1995;269:1737–1740.
35. Niethammer M, Kim E, Sheng M. Interaction between the C terminus of NMDA receptor subunits and multiple members of the PSD-95 family of membrane-associated guanylate kinases. *J Neurosci*. 1996;16:2157–2163.
36. Won S, Incontro S, Nicoll RA, Roche KW. PSD-95 stabilizes NMDA receptors by inducing the degradation of STEP61. *Proc Natl Acad Sci U S A*. 2016;113:E4736–E4744.
37. Freund WD, Reddig S. AMPA/Zn(2+)-induced neurotoxicity in rat primary cortical cultures: Involvement of L-type calcium channels. *Brain Res*. 1994;654:257–264.
38. Koh JY, Choi DW. Zinc toxicity on cultured cortical neurons: Involvement of N-methyl-D-aspartate receptors. *Neuroscience*. 1994;60:1049–1057.
39. Yin HZ, Weiss JH. Zn(2+) permeates Ca(2+) permeable AMPA/kainate channels and triggers selective neural injury. *Neuroreport*. 1995;6:2553–2556.
40. Harper S, Speicher DW. Purification of proteins fused to glutathione S-transferase. *Methods Mol Biol (Clifton, NJ)*. 2011;681:259–280.
41. Bornhorst JA, Falke JJ. Purification of proteins using polyhistidine affinity tags. *Methods Enzymol*. 2000;326:245–254.
42. Farrow NA, Muhandiram R, Singer AU, et al. Backbone dynamics of a free and phosphopeptide-complexed Src homology 2 domain studied by 15N NMR relaxation. *Biochemistry*. 1994;33:5984–6003.
43. Summers MF, Henderson LE, Chance MR, et al. Nucleocapsid zinc fingers detected in retroviruses: EXAFS studies of intact viruses and the solution-state structure of the nucleocapsid protein from HIV-1. *Protein Sci*. 1992;1:563–574.
44. Wang B, Alam SL, Meyer HH, et al. Structure and ubiquitin interactions of the conserved zinc finger domain of Npl4. *J Biol Chem*. 2003;278:20225–20234.
45. Zhang Y, Larsen CA, Stadler HS, Ames JB. Structural basis for sequence specific DNA binding and protein dimerization of HOXA13. *PLoS One*. 2011;6:e23069.
46. Williamson MP. Using chemical shift perturbation to characterise ligand binding. *Prog Nucl Magn Reson Spectrosc*. 2013;73:1–16.
47. Chowdhury D, Hell JW. Ca(2+)/calmodulin binding to PSD-95 downregulates its palmitoylation and AMPARs in long-term depression. *Front Synaptic Neurosci*. 2019;11:6.

**How to cite this article:** Zhang Y, Fang X, Ascota L, Li L, Guerra L, Vega A, et al. Zinc-chelating postsynaptic density-95 N-terminus impairs its palmitoyl modification. *Protein Science*. 2021;30:2246–57. <https://doi.org/10.1002/pro.4187>